Importance of Charge Fluctuations for the Topological Phase in SmB_6

Chul-Hee Min,[1,2,*] P. Lutz,[1] S. Fiedler,[1,2] B. Y. Kang,[3] B. K. Cho,[3,†] H.-D. Kim,[4,5] H. Bentmann,[1,2] and F. Reinert[1,2]
[1]Universität Würzburg, Experimentelle Physik VII, 97074 Würzburg, Germany
[2]Karlsruhe Institut für Technologie KIT, Gemeinschaftslabor für Nanoanalytik, 76021 Karlsruhe, Germany
[3]School of Materials Science and Engineering, Gwangju Institute of Science and Technology (GIST), Gwangju 500-712, Republic of Korea
[4]Center for Correlated Electron Systems, Institute for Basic Science (IBS), Seoul 151-747, Republic of Korea
[5]Department of Physics and Astronomy, Seoul National University, Seoul 151-747, Republic of Korea
(Received 24 February 2014; published 5 June 2014)

Typical Kondo insulators (KIs) can have a nontrivial $\mathbb{Z}_2$ topology because the energy gap opens at the Fermi energy (E_F) by a hybridization between odd- and even-parity bands. SmB_6 deviates from such KI behavior, and it has been unclear how the insulating phase occurs. Here, we demonstrate that charge fluctuations are the origin of the topological insulating phase in SmB_6. Our angle-resolved photoemission spectroscopy results reveal that with decreasing temperature the bottom of the d-f hybridized band at the $\bar{X}$ point, which is predicted to have odd parity and is required for a topological phase, gradually shifts from below to above E_F. We conclude that SmB_6 is a charge-fluctuating topological insulator.

DOI: 10.1103/PhysRevLett.112.226402 PACS numbers: 71.28.+d, 71.20.−b, 71.27.+a, 79.60.−i

After "topology" was found to be a fundamental concept for the description of the electronic properties of solids [1–3], especially including strongly correlated systems [4], samarium hexaboride (SmB_6) has drawn much attention as it might represent a unique class of condensed matter called a topological Kondo insulator [4,5]. The energy gap of conventional Kondo insulators (KIs) [6–8] opens at the Fermi energy (E_F) because of the hybridization between a renormalized f band and a conduction d band. This gap opening happens typically below the coherence temperature where spin rather than charge fluctuations play the major role [9–11]. KIs can have a nontrivial $\mathbb{Z}_2$ topology [4] because the odd-parity f band shifts above E_F and gives rise to a band inversion, i.e., a change in the $\mathbb{Z}_2$ topological indices [12,13]. Such a nontrivial topological phase with topologically protected surface states can explain the characteristic constant resistivity region at $T < 5$ K in SmB_6 [5,14–17].

However, SmB_6 deviates from a conventional KI [18] because its gap is insensitive to doping and pressure [11,19–22]. The origin of this difference and the band inversion remains unclear. Despite extensive experimental and theoretical investigations on SmB_6, the electronic structure and its connection to the temperature dependence are not fully understood up to now—mainly because of the complex interplay between strong electron correlations, spin-orbit interaction, and multiplet splitting. We present here a detailed experimental approach by high-resolution angle-resolved photoemission spectroscopy (ARPES) with the focus on the temperature dependence of surface and bulk electronic structure.

Figure 1 shows the general electronic structure of SmB_6. Figure 1(a) on the left gives the surface Brillouin zone of SmB_6 with elliptical Fermi surface (FS) sheets around the $\bar{X}$ points. The experiments were carried out at the UE112-PGM-1b ("1^3") beam line of BESSY II using $h\nu = 70$ eV at 3 K $\leq T \leq$ 108 K at Helmholtz-Zentrum Berlin (HZB) (see also the Supplemental Material [23]). The details of the electronic structure are analyzed along the white dashed lines (i) and (ii), corresponding to the high symmetry lines $\bar{M}$–$\bar{X}$ and $\bar{X}$–$\bar{\Gamma}$, respectively. Figure 1(b) shows the ARPES intensity as a function of binding energy E_B (y axis) and momentum $k_\parallel$ (x axis) along $\bar{M}$–$\bar{X}$ at low temperatures, i.e., at $T = 3$ K. The surface state $S1$ (green dashed line) [32,33] crosses E_F and forms the observed elliptic sheets in the FS plots in Fig. 1(a). The Sm $4f$ states appear in the photoemission data as final-state multiplets for the $f^6 \rightarrow f^5$ transition. The right sides of Figs. 1(b) and 1(c) show the integrated energy distribution curves (EDCs) together with black bars, which denote the calculated relative intensities and energy positions of the ${}^6H_{5/2}$, ${}^6H_{7/2}$, and ${}^6F$ contributions [34–36]. In the angle-resolved data, the multiplets appear as narrow bands that hybridize with the bulk d band $B1$ [32,33], clearly visible by a changing slope of $B1$ within the three displayed energy regions. Such a hybridization is only possible if the multiplets have the same symmetry as $B1$, leading to hybridization gaps between $B1$ and the narrow $4f$ bands [21].

In order to investigate the temperature-dependent development of the gap, we performed ARPES measurements along $\bar{X}$–$\bar{\Gamma}$ [Fig. 2(a)] for various temperatures. At an intermediate temperature of $T = 60$ K, one can observe a lower ($B1$, marked black) and an upper quasiparticle band ($B2$, blue). At this temperature, the upper band $B2$ appears around $\bar{X}$ with a maximum binding energy slightly below E_F, but it gradually vanishes with decreasing temperature.

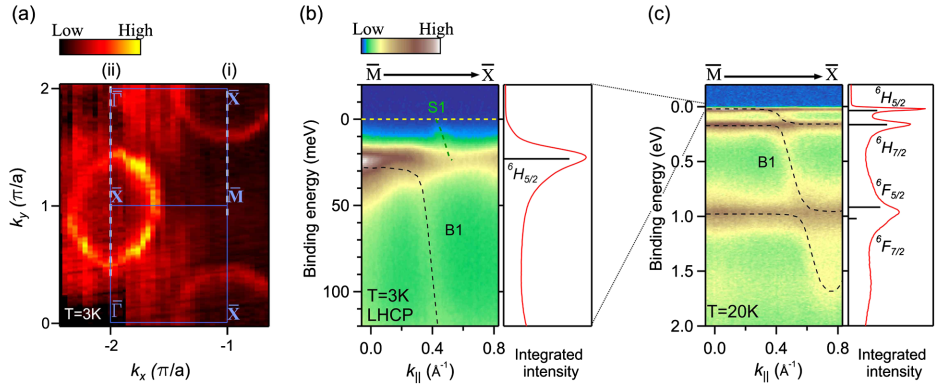

FIG. 1 (color online). Overview of the electronic structure of SmB_6. (a) FS map of SmB_6 obtained at $T = 3$ K using $h\nu = 70$ eV. Elliptical FS sheets appear around the $\bar{X}$ points. ARPES spectra were obtained along the white lines (i) and (ii) representing the high-symmetry directions $\bar{M}$–$\bar{X}$, and $\bar{X}$–$\bar{\Gamma}$. (b), left: ARPES intensity vs binding energy (E_B) and momentum ($k_{||}$) along (i). The surface state $S1$ [32,33] is indicated by the green dashed line and crosses E_F ($E_B = 0$). The bulk- quasiparticle band $B1$ is indicated by black dashed lines. (b), right: integrated EDC from the data on the left. The $^6H_{5/2}$ final state multiplet is positioned at $E_B = 21$ meV. (c), left: wide energy range ARPES spectrum measured along (i). As illustrated with black dashed lines, $B1$ does not show a simple parabolic dispersion [32,33] because its slope changes due to hybridization with the $^6H_{5/2}$, $^6H_{7/2}$, and ^6F final state multiplets for the $f^6 \rightarrow f^5$ transitions. (c), right: integrated EDC from the left with calculated multiplet lines [34].

As a consequence, the density of states at E_F decreases, as shown in the angle-integrated EDC in Fig. 2(b). In addition, one can observe that the dominating peak of the $^6H_{5/2}$ multiplet increases in intensity and decreases in width with decreasing temperature [7,8]. The narrowing of the $4f$ features results in well-developed quasiparticle bands and, thus, indicates that the temperature approaches the coherence temperature. In order to investigate the spectra near E_F up to an energy of $\approx 5k_BT$ above E_F, we divided the integrated spectra by the Fermi-Dirac distribution [Fig. 2(c)] [37]. Through this well-established normalization, we are able to see that $B2$, leading to a characteristic intensity slightly above E_F, shifts from below to above E_F with decreasing temperature. On the other hand, the intensity of the strong $^6H_{5/2}$ peak increases, which implies that the spectral weight of $B2$ is mainly redistributed to this $4f$ feature when it disappears from the gap region at E_F. The temperature dependence of the gap region is shown in the inset of Fig. 2(c): at $T = 60$ K the gap is filled because $B2$ crosses E_F, at 40 K the gap opens, and at low temperatures E_F shifts towards the middle of the gap. The schematic diagram in Fig. 2(d) illustrates the observed band structure in Fig. 2(a) and the energy shifts of $B1$ and $B2$ with respect to E_F.

To investigate the behavior of $B2$ in more detail, we took momentum distribution curves (MDCs) from the ARPES data in the range $|E_B| \leq 8$ meV [Fig. 2(e)]. Between the two $S1$ peaks (green bars), considerable spectral weight of $B2$ is present near E_F, indicated by the blue striped area. The area is drawn as a guide to the eye using U-shaped background lines extracted from MDC at higher E_B. With decreasing temperature below 60 K, the spectral weight of $B2$ below E_F is reduced. Moreover, the two peaks due to $B2$ at E_F (cyan bars) approach each other. This indicates that $B2$ gradually shifts above E_F as sketched in Fig. 2(d). Therefore, the gap evolution of SmB_6 deviates from that of a conventional KI whose gap starts to open right at E_F. At $T = 3$ K, there remains a small finite weight that possibly originates from the incoherent part of $B2$ or from the predicted topological surface states (TSSs) [12,13,38].

The overall band structure near E_F observed in our ARPES spectra consisting of the lower and upper d-f hybridized bands $B1$ and $B2$ is in agreement with the predictions from *ab initio* and model-based theoretical approaches [12,13,38]. In addition, the proposed scheme in Fig. 2(d) is further substantiated by the reduction of spectral weight of the $4f$ band ($^6H_{5/2}$) around the $\bar{X}$ point. Therefore, we consider $B2$ as a bulk-derived feature. The determined gap evolution is in agreement with crucial features in the physical properties of SmB_6 above 30 K. The steep slope in resistivity at $T = 40$ K, the maximum number of electron carriers at $T = 57$ K detected in Hall measurements [39,40], and the broad peak in the heat capacity at $T \approx 40$ K [41] can be understood as the consequence of the shift of the bulk band $B2$, which leads to the unusual (semi)metal-insulator phase transition [39]. Furthermore, the shift can explain the significant change in f electron density occurring at $T > 30$ K in x-ray absorption data [42].

Since the $4f$ states are located near E_F in mixed valence systems [21,22] as SmB_6, thermally excited charge fluctuations between localized f and itinerant d states determine the thermodynamic properties [9]. The influence of charge fluctuations on the electronic structure near E_F is observed in our data by the shift of $B2$ and the spectral weight redistribution. The shift reflects the change in the

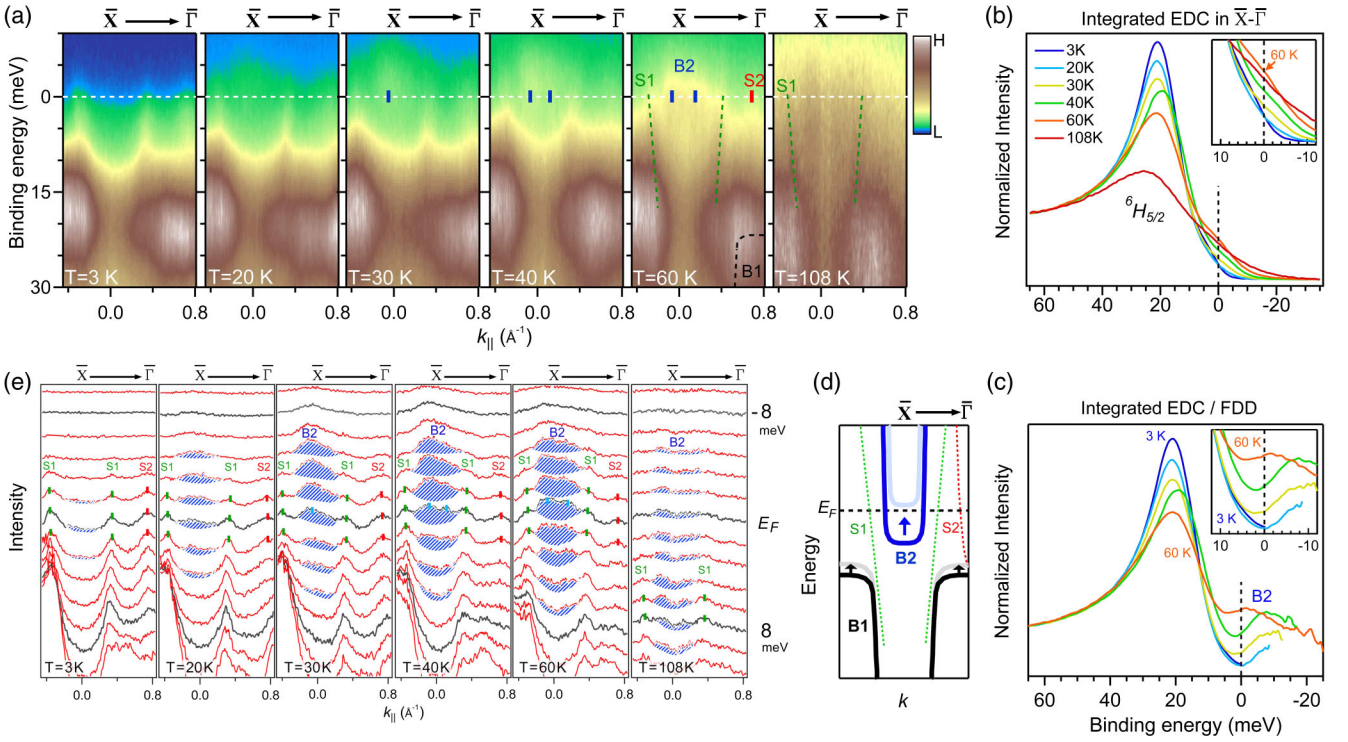

FIG. 2 (color online). Gap evolution in the $\bar{X}$–$\bar{\Gamma}$ direction. (a) Temperature dependence of the ARPES data (vs E_B and $k_{\|}$). A lower and an upper quasiparticle band $B1$ [32,33] and $B2$ are indicated in black and blue; the surface states $S1$ and $S2$ [32,33] are indicated in green and red, respectively. At the $\bar{X}$ point, $B2$ appears below E_F at $T \geq 60$ K and gradually vanishes with decreasing temperature. (b) Temperature-dependent integrated EDC between the $\bar{X}$ and $\bar{\Gamma}$ points in (a). The $^6H_{5/2}$ final state multiplet develops with decreasing temperature. Inset in (b): the EDC at $T = 60$ K has the highest spectral weight at E_F. (c) EDC for 3 K $\leq T \leq$ 60 K divided by the Fermi-Dirac distribution (FDD). $B2$ shifts from below to above E_F. Inset in (c): enlarged spectra near E_F. At $T = 60$ K E_F is positioned at the bottom of $B2$, and with further decreasing temperature it shifts to the middle of the gap. (d) Schematic energy-band diagram illustrating the observed band structure in (a). The energy shifts of $B1$ and $B2$ with decreasing temperature are indicated by arrows. (e) MDCs taken from the data in (a) close to E_F. Bars indicate the peak positions for $B2$, $S1$, and $S2$ with the specific colors. The blue striped areas denote the spectral weight of $B2$. The spectral weight of $B2$ close to E_F reduces for $T < 60$ K. The intensity of $B2$ becomes narrower with decreasing temperature, indicating that $B2$ gradually shifts upwards.

carrier density [40] and the increase in the localized f electron density [42]. Thus, our results give a microscopic explanation for the unique temperature dependence of the physical properties of SmB_6 and clearly indicate that charge fluctuations play the major role in the phase transition of SmB_6 so that at $T > 30$ K it belongs to the charge fluctuation regime of the Anderson model [10,11].

Another important aspect follows from the fact that $B2$ is expected to have odd parity at the X point and lies above E_F in the ground state. This means that SmB_6 is in a strong topological insulator phase with odd $\mathbb{Z}_2$ topological invariants [12,13,38]. Therefore, we investigated the electronic structure for signatures of a nontrivial topological phase, which would be proven by the existence of TSSs. In fact, we observe three different surface states: $S1$ at the $\bar{X}$ point [32,33,43], $S2$ at the $\bar{\Gamma}$ point [32,33], and the new state $S3$ also at the $\bar{X}$ point. The surface states $S1$ and $S2$ indicated in green and red, respectively (Fig. 2), are located near E_F. $S2$ has been theoretically proposed to be a TSS [12,13,38] whereas $S1$ has not been predicted yet. $S1$ might be a surface band originating from the Sm ions at the surface having a different valence from that in the bulk [44] or from other surface reconstructions [28,45,46].

In addition to the states $S1$ and $S2$, our data show the existence of a Dirac-cone-like band $S3$ at $E_B = 20$ meV and $\bar{X}$, as predicted by a renormalized band calculation [38] [Fig. 3(a)]. The red and blue lines represent the TSSs and bulk bands projected on the (001) surface, respectively. In order to separate dispersive bands from k-independent features [21] in Figs. 3(b) and 3(c), the ARPES intensity is plotted on a normalized logarithmic scale along $\bar{M}$–$\bar{X}$ and compared with the theoretical band structure. The calculated band structure has to be shrunk in energy to match $B1$ hybridizing with the $^6H_{5/2}$ feature. By circular dichroism in the photoemission process [Figs. 3(b) and 3(c), left], one of the two bands (red circles) crossing at the $\bar{X}$ point is separately enhanced, which is a typical dichroism behavior for spin-helical Dirac cones [27]. These bands $S3$ are in reasonable agreement with calculated surface states [red lines in Fig. 3(a)] (see also the Supplemental Material [23]).

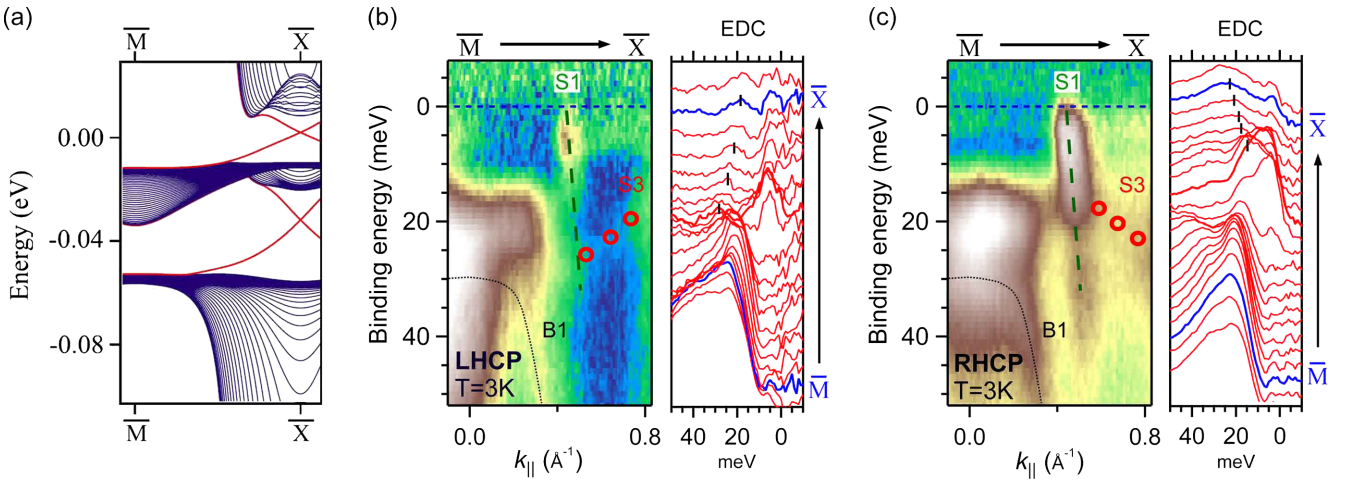

FIG. 3 (color online). Band structure along $\bar{M}$–$\bar{X}$. (a) Calculated projected bulk band structures and surface states on the (001) surface from Ref. [15]. The blue and red lines are the projected bulk bands and the topological surface states, respectively. (b) and (c), left: ARPES intensity maps along $\bar{M}$–$\bar{X}$ on a logarithmic intensity scale. Depending on the helicity of the circularly polarized light, one branch (red circles) of surface state $S3$ is selectively enhanced in intensity. Compared to the theoretical calculation, bands $S3$ could be topological surface states. (b) and (c), right: respective EDC cuts from the data on the left.

The corresponding EDCs [Figs. 3(b) and 3(c), right] further confirm the existence of the Dirac-cone-like bands, which appear as dispersing peaks marked by black lines.

The comparison of the theoretical and experimental band structure given in Fig. 3 confirms that bands $S3$ disperse as the predicted TSSs that appear within the local gap region of the projected bulk band structure—in addition to $S2$ [32,33]. Thus, SmB_6 can be in the strong topological phase as predicted [38,47] because the odd-parity band $B2$ is positioned above E_F at the X point corroborated by our results [46]. As has been demonstrated, the states at E_F are strongly influenced by charge fluctuations, which drive the position of E_F into the middle of the gap and are responsible for the band inversion that eventually makes SmB_6 different from a conventional KI. Our finding indicates that the energy gap of SmB_6 is rather a charge gap than a spin gap as in a typical KI, which is larger in size and less sensitive to doping and pressure [11,19–22]. Moreover, the coherence temperature is higher in the charge fluctuation regime, so the quantum spin Hall state is possibly accessible with transport measurements at higher temperature as demonstrated already theoretically [11]. Therefore, mixed valence insulators can be candidates to realize spin polarized currents in a high possible temperature range.

We acknowledge F. Assaad, J. Werner, J. Kroha, S.-J. Oh, E.-J Cho, B.-J. Yang, and J. Allen for helpful discussions. C.-H. M. thanks E. Rienks, F. Boariu, and H. Schwab for assistance during the beam time and also J. Y. Kim and S. S. Lee for the initial characterization. This research was supported by the Deutsche Forschungsgemeinschaft (Grant No. FOR1162), HZB, National Research Foundation of Korea (NRF) Grants funded by the Korean government (MSIP) (No. 2011-0028736, No. 2008-0062606, and No. 2013K000315), and the Institute for Basic Science (IBS) in Korea.

*Corresponding author.
cmin@physik.uni-wuerzburg.de
†Corresponding author.
chobk@gist.ac.kr

[1] J. E. Moore, Nature (London) **464**, 194 (2010).
[2] L. Fu and C. L. Kane, Phys. Rev. B **76**, 045302 (2007).
[3] M. Z. Hasan and C. L. Kane, Rev. Mod. Phys. **82**, 3045 (2010).
[4] M. Dzero, K. Sun, V. Galitski, and P. Coleman, Phys. Rev. Lett. **104**, 106408 (2010).
[5] S. Wolgast, Ç. Kurdak, K. Sun, J. W. Allen, D.-J. Kim, and Z. Fisk, Phys. Rev. B **88**, 180405 (2013).
[6] P. S. Riseborough, Adv. Phys. **49**, 257 (2000).
[7] S. Nozawa, T. Tsukamoto, K. Kanai, T. Haruna, S. Shin, and S. Kunii, J. Phys. Chem. Solids **63**, 1223 (2002).
[8] S. Souma, H. Kumigashira, T. Ito, T. Takahashi, and S. Kunii, Physica (Amsterdam) **312B–313B**, 329 (2002).
[9] A. C. Hewson, *The Kondo Problem to Heavy Fermions* (Cambridge University Press, Cambridge, England, 1993).
[10] P. Coleman, *Introduction to Many Body Physics* (Cambridge University Press, Cambridge, England, 2011).
[11] J. Werner and F. F. Assaad, arXiv:1311.3668.
[12] T. Takimoto, J. Phys. Soc. Jpn. **80**, 123710 (2011).
[13] V. Alexandrov, M. Dzero, and P. Coleman, Phys. Rev. Lett. **111**, 226403 (2013).
[14] D. J. Kim, T. Grant, and Z. Fisk, Phys. Rev. Lett. **109**, 096601 (2012).
[15] S. Yeo, K. Song, N. Hur, Z. Fisk, and P. Schlottmann, Phys. Rev. B **85**, 115125 (2012).

[16] D. J. Kim, S. Thomas, T. Grant, J. Botimer, Z. Fisk, and J. Xia, Sci. Rep. **3**, 3150 (2013).
[17] Y. Nakajima, P. S. Syers, X. Wang, R. Wang, and J. Paglione, arXiv:1312.6132.
[18] T. Pietrus, H. v. Löhneysen, and P. Schlottmann, Phys. Rev. B **77**, 115134 (2008).
[19] J. C. Cooley, M. C. Aronson, Z. Fisk, and P. C. Canfield, Phys. Rev. Lett. **74**, 1629 (1995).
[20] M. Kasaya, H. Kimura, Y. Ishikawa, T. Fujita, and T. Kasuya, in *Valence Fluctuations in Solids*, edited by L. M. Falicov, W. Hanke, and M. B. Maple (North-Holland, Amsterdam, 1981) p. 251.
[21] R. M. Martin and J. W. Allen, J. Appl. Phys. **50**, 7561 (1979).
[22] C. M. Varma, Rev. Mod. Phys. **48**, 219 (1976).
[23] See the Supplemental Material at http://link.aps.org/supplemental/10.1103/PhysRevLett.112.226402, which includes Refs. [24–31].
[24] S. V. Borisenko, Synchrotron Radiat. News **25**, 6 (2012).
[25] N. N. Sirota, V. V. Novikov, V. A. Vinokurov, and Y. B. Paderno, Phys. Solid State **40**, 1856 (1998).
[26] H. Miyazaki, T. Hajiri, T. Ito, S. Kunii, and S. I. Kimura, Phys. Rev. B **86**, 075105 (2012).
[27] Y. Wang and N. Gedik, Phys. Status Solidi RRL **7**, 64 (2013).
[28] Z.-H. Zhu, A. Nicolaou, G. Levy, N. P. Butch, P. Syers, X. F. Wang, J. Paglione, G. A. Sawatzky, I. S. Elfimov, and A. Damascelli, Phys. Rev. Lett. **111**, 216402 (2013).
[29] V. B. Zabolotnyy, S. V. Borisenko, A. A. Kordyuk, D. S. Inosov, A. Koitzsch, J. Geck, J. Fink, M. Knupfer, B. Büchner, S.-L. Drechsler, V. Hinkov, B. Keimer, and L. Patthey, Phys. Rev. B **76**, 024502 (2007).
[30] M. R. Scholz, J. Sánchez-Barriga, J. Braun, D. Marchenko, A. Varykhalov, M. Lindroos, Y. J. Wang, H. Lin, A. Bansil, J. Minár, H. Ebert, A. Volykhov, L. V. Yashina, and O. Rader, Phys. Rev. Lett. **110**, 216801 (2013).
[31] S. R. Park, J. Han, C. Kim, Y. Y. Koh, C. Kim, H. Lee, H. J. Choi, J. H. Han, K. D. Lee, N. J. Hur, M. Arita, K. Shimada, H. Namatame, and M. Taniguchi, Phys. Rev. Lett. **108**, 046805 (2012).
[32] N. Xu, X. Shi, P. K. Biswas, C. E. Matt, R. S. Dhaka, Y. Huang, N. C. Plumb, M. Radović, J. H. Dil, E. Pomjakushina, K. Conder, A. Amato, Z. Salman, D. M. Paul, J. Mesot, H. Ding, and M. Shi, Phys. Rev. B **88**, 121102 (2013).
[33] J. Jiang, S. Li, T. Zhang, Z. Sun, F. Chen, Z. R. Ye, M. Xu, Q. Q. Ge, S. Y. Tan, X. H. Niu, M. Xia, B. P. Xie, Y. F. Li, X. H. Chen, H. H. Wen, and D. L. Feng, Nat. Commun. **4**, 3010 (2013).
[34] F. Gerken, J. Phys. F **13**, 703 (1983).
[35] J. N. Chazalviel, M. Campagna, G. K. Wertheim, and P. H. Schmidt, Phys. Rev. B **14**, 4586 (1976).
[36] J. Denlinger, G.-H. Gweon, J. Allen, C. Olson, Y. Dalichaouch, B.-W. Lee, M. Maple, Z. Fisk, P. Canfield, and P. Armstrong, Physica (Amsterdam) **281B–282B**, 716 (2000).
[37] D. Ehm, F. Reinert, S. Schmidt, G. Nicolay, S. Hüfner, J. Kroha, O. Trovarelli, and C. Geibel, Physica B (Amsterdam) **312B–313B**, 663 (2002).
[38] F. Lu, J. Z. Zhao, H. Weng, Z. Fang, and X. Dai, Phys. Rev. Lett. **110**, 096401 (2013).
[39] J. C. Nickerson, R. M. White, K. N. Lee, R. Bachmann, T. H. Geballe, and G. W. Hull, Phys. Rev. B **3**, 2030 (1971).
[40] J. W. Allen, B. Batlogg, and P. Wachter, Phys. Rev. B **20**, 4807 (1979).
[41] E. V. Nefedova, P. A. Alekseev, V. N. Lazukov, and I. P. Sadikov, J. Exp. Theor. Phys. **96**, 1113 (2003).
[42] M. Mizumaki, S. Tsutsui, and F. Iga, J. Phys. Conf. Ser. **176**, 012034 (2009).
[43] M. Neupane, N. Alidoust, S.-Y. Xu, T. Kondo, D.-J. Kim, C. Liu, I. Belopolski, T.-R. Chang, H.-T. Jeng, T. Durakiewicz, L. Balicas, H. Lin, A. Bansil, S. Shin, Z. Fisk, and M. Z. Hasan, arXiv:1306.4634.
[44] M. Aono, R. Nishitani, C. Oshima, T. Tanaka, E. Bannai, and S. Kawai, Surf. Sci. **86**, 631 (1979).
[45] S. Rößler, T.-H. Jang, D. J. Kim, L. H. Tjeng, Z. Fisk, F. Steglich, and S. Wirth, Proc. Natl. Acad. Sci. U.S.A. **111**, 4798 (2014).
[46] J. D. Denlinger, J. W. Allen, J.-S. Kang, K. Sun, J.-W. Kim, J. H. Shim, B. I. Min, D.-J. Kim, and Z. Fisk, arXiv:1312.6637.
[47] C.-J. Kang, J. Kim, K. Kim, J.-S. Kang, J. D. Denlinger, and B. I. Min, arXiv:1312.5898.